Макрогетероциклы
http://mhc-isuct.ru

DOI: 10.6060/mhc235502g

Probing the Conformational Space and Molecular Structure of 5,10,15,20-Tetraphenyl-21H,23H-Porphyrin – Reference Point for Tetraphenylporphyrin Metal Complexes

Ivan Yu. Kurochkin,[a] Nina I. Giricheva,[b] Alexander V. Krasnov,[a] Alexey N. Kiselev,[a,c] and Georgiy V. Girichev[a@]

[a]*Ivanovo State University of Chemistry and Technology, 153000 Ivanovo, Russia*
[b]*Nanomaterial Research Institute, Ivanovo State University, 153025 Ivanovo, Russia*
[c]*G.A. Krestov Institute of Solution Chemistry of RAS, 153045 Ivanovo, Russia*
[@]*Corresponding author E-mail: girichev@isuct.ru*

Gas-phase electron diffraction and quantum chemical study of the isolated H_2TPP molecule was carried out, which can be considered as a reference point for tetraphenylporphyrin metal complexes. Using Knudsen effusion mass spectrometry, the enthalpy of sublimation of the H_2TPP was determined to be 212(4) kJ/mol (535 K). Using DFT/B97D/cc-pVTZ in combination with gas electron diffraction it is shown that the saturated vapor of H_2TPP consists of a mixture of conformers. The conformers differ in the mutual orientation of the four phenyl fragments relative to each other and have close energies. Bond lengths and bond angles in conformers were determined. NBO analysis showed a change in the delocalization of the electron density between the phenyl substituents and the macroheterocyclic (MHC) skeleton with a change in the torsion angle. This delocalization is the reason for the non-orthogonal position of phenyl meso-substituents in the conformers of H_2TPP and other tetraphenyl substituted porphyrins. Non-covalent interactions between the MHC skeleton and phenyl substituents have been described using the FI-SAPT0 method. The change in geometric and electronic characteristics in the series of molecules H_2P, H_2TPP, H_2FTPP, ZnTPP and PdTPP is considered. Based on Valence Shell Electron Pair Repulsion (VSEPR) theory, an explanation is given for the influence of the substituent on the parameters of the MHC skeleton. Analysis of changes in the energy of frontier orbitals in the indicated series of molecules makes it possible to predict the direction of changes in the red-ox properties of compounds with various modifications of H_2TPP.

Keywords: Tetraphenylporphyrin, metal tetraphenylporphyrins, molecular structure, sublimation enthalpy, conformers.

Исследование конформационного многообразия и молекулярной структуры 5,10,15,20-тетрафенил-21H,23H-порфирина – отсчетной точки для тетрафенилпорфириновых металлокомплексов

И. Ю. Курочкин,[a] Н. И. Гиричева,[b] А. В. Краснов,[a] А. Н. Киселев,[a,c] Г. В. Гиричев[a@]

[a]*Ивановский государственный химико-технологический университет, 153000 Иваново, Россия*
[b]*Научно-исследовательский институт наноматериалов Ивановского государственного университета, 153025 Иваново, Россия*
[c]*Институт химии растворов имени Г.А. Крестова РАН; 153045 Иваново, Россия*
[@]*E-mail: girichev@isuct.ru*

Проведено электронографическое и квантово-химическое исследование свободной от коллективного взаимодействия молекулы H_2TPP, структуру которой можно рассматривать как отсчетную точку для тетрафенилпорфириновых металлокомплексов. С помощью эффузионной масс-спектрометрии Кнудсена

определена энтальпия сублимации H_2TPP, которая оказалась равной 212(4) кДж/моль (535 К), что позволило устранить противоречия для данной характеристики в литературе. Показано, что соединение H_2TPP термически устойчиво, по крайней мере, до 660 К. Состав ионов в масс-спектре не меняется с повышением температуры и все ионы имеют единственного молекулярного предшественника, H_2TPP. С помощью метода DFT/B97D/cc-pVTZ в сочетании с газовой электронографией (T=657 К) показано, что насыщенный пар H_2TPP состоит из смеси конформеров, которые различаются взаимной ориентацией четырех фенильных фрагментов друг относительно друга и имеют близкие энергии. Определены длины связей и валентные углы в конформерах. NBO-анализ показал характер изменения делокализации электронной плотности между фенильными заместителями и остовом макрогетероцикла при изменении торсионного угла. Эта делокализация является причиной неортогонального положения фенильных мезозаместителей в конформерах H_2TPP и других тетрафенилзамещенных порфиринах. Нековалентные взаимодействия между макогетероциклическим остовом и фенильными заместителями описаны с помощью метода FI-SAPT0. Установлено, что молекула H_2TPP характеризуется конформационной нежесткостью и может рассматриваться как отсчетная точка при сравнении структуры соединений, полученных введением атома металла в координационную полость или заместителей по периферии макрогетероциклического остова. Рассмотрено изменение геометрических и электронных характеристик в ряду молекул H_2P, H_2TPP, H_2FTPP, ZnTPP и PdTPP. На основе теории отталкивания электронных пар валентной оболочки (ТОЭПВО) дано объяснение влияния заместителя на параметры остова макрогетероцикла. Анализ изменения энергии граничных орбиталей в указанном ряду молекул позволяет прогнозировать направление изменения окислительно-восстановительных свойств соединений при различных модификациях H_2TPP.

Ключевые слова: Тетрафенилпорфирин, металлотетрафенилпорфирины, молекулярная структура, энтальпия сублимации, конформеры.

Introduction

Macroheterocyclic complexes based on pyrrole and isoindole represent one of the most important classes of organic compounds. Their stability, wide possibilities for modifying the periphery, and the ability to form complexes with various metals have made these complexes the central objects in a large number of studies, both fundamental and applied (see, for example,[1-5]).

Tetraphenylporphyrin H_2TPP is the predecessor of metal-free macroheterocyclic compounds of the H_2TXPP type and MTXPP metal complexes, which have a wide range of physicochemical properties in which one or more hydrogen atoms in the phenyl substituents are replaced by functional groups X of different nature. By varying X, one can achieve the desired changes in the properties of the compound, ranging from changing porphyrin acidity[6] to creating synthons used to construct porous metal-organic framework structures.[7]

H_2TPP can be considered as a reference compound when comparing the physicochemical properties of compounds created by introducing substituents into the phenyl rings and skeleton of the molecule. Knowledge of the structure of H_2TPP in the condesed state (when collective interactions occur),[8-16] and in the gaseous state (molecules free from collective interaction) allows one to interpolate, predict and explain changes in the structure and a number of physicochemical properties under the influence of external factors, for example, solvent.[17]

The crystal structure of H_2TPP was studied in [8–16]. In an early work,[8] the crystal structure was classified as tetragonal (Table S1, *Supporting Information*). However, a large value of the disagreement factor (R_F>10%) indicated the low accuracy of the result obtained.[8] Later, in a series of works,[9–16] consistent data were obtained indicating a slight distortion of the symmetry of C_{2h}(1) molecules due to intermolecular interaction (Figure 1) and crystal possesses triclinic syngonia (Figure S1, Table S1). In H_2TPP molecules, four phenyl *meso*-substituents are deviated from a position perpendicular to the macroheterocyclic (MHC) plane, which ensures close packing of the crystal with the shortest distances of ~2.9 Å between the phenyl fragment of one molecule and the frame of the nearest molecule, and ~3.2 Å between the phenyl fragments of neighboring molecules. When the temperature increases from 100 K[13-16] to room temperature,[10-12] the structure of the molecule in the crystallographic cell is maintained, and the torsion angle θ between the plane of the phenyl substituent and the MHC skeleton increases from ~60° to ~62°, the packing density decreases from 1.31 to 1.28 and the molecular volume increases from 779 to 800 Å^3 (Table S1). Deviation of the angle θ from 90° leads to noticeable non-planarity of the MHC skeleton in crystal structures.

Based on the concept of steric interaction between phenyl fragments and MHC skeleton, it can be assumed that the most favorable structure of H_2TPP will be the structure of D_{2h} symmetry with a planar macroheterocycle and phenyl substituents oriented perpendicular to it (Figure 1). Therefore, the question arises: is the rotation of the phenyl fragments from a position perpendicular to the MHC plane a structural feature of the individual H_2TPP molecule or a consequence of intermolecular interactions in the crystal.[8-16] To answer this question, it is necessary to determine the structure of free molecule existing in the gas phase.

To date, an experimental study of the molecular structure in the gaseous state of only three representatives of tetraphenylporphines has been carried out – metal-free 5,10,15,20-tetrakis(4′-fluorophenyl)porphyrin (H_2TFPP),[18]

and metal complexes 5,10,15,20-tetraphenylporphyrinatozinc(II) and palladium(II) (ZnTPP and PdTPP),[19] the structure of which is interesting to compare with the structure of H_2TPP in order to trace the change in the structure of the reference compound that occurs when a metal atom is introduced into the coordination cavity or a substituent into the phenyl fragments.

Works[18,19] show that metal-free H_2TFPP and metal complexes ZnTPP and PdTPP have high thermal stability and volatility at temperatures about 550 K and can be used in technologies involving the gas-phase state. The formation of thin porphyrin films with needed structure and chemical composition is usually performed by physical vapor deposition (PVD) or chemical vapor deposition (CVD) technologies. To understand the physicochemical processes occurring during the formation of films and coatings, reliable information is needed on the heat of vaporization, the composition of the gas phase and the structure of the molecular forms present in the vapor.

The data on the thermodynamics of H_2TPP sublimation existing in the literature cannot be called reliable. The enthalpy of sublimation of H_2TPP was determined 8 times by different tensimetric methods.[20-27] The resulting value turned out to be very uncertain and varied from 115 to 240 kJ/mol. Therefore, one of the goals of our work was to determine the enthalpy of sublimation for this compound.

Works[28-30] show that the actual conformational and regioisomeric composition of MHC metal complexes and their reactivity depend not only on the nature of the central metal atom, but are also determined by the structural features of the substituents in the MHC skeleton. In this regard, the main goal of this work is to determine the geometric structure of the H_2TPP molecule, free from collective interaction, and to consider the factors influencing the features of its structure, as a reference point in systematizing the structures of metal complexes and metal-free tetraphenylporphyrins with various substituents along the periphery of the macrocycle.

The presented in our work material was obtained using the Knudsen effusion method with mass spectrometric control of the vapor composition, synchronous electron diffraction/mass spectrometric experiment (GED/MS) and quantum chemical calculations (QC) and may be in demand in the design of new materials to assess the influence of one or another type of substitution along the periphery and/or in coordination center.

Experimental

Computational details

The geometry optimization of all H_2TPP molecular forms was performed within the framework of DFT with using of B3LYP[31-33] and B97D[34] functionals. Danning basis set *cc-pVTZ*[35] was used for H, C, N atoms. Vibrational frequencies were calculated for all the optimized structures to characterize the stationary points. The electron density distribution was analyzed using the NBO program[36] from the Gaussian09 software.[37]

DFT calculated geometrical parameters and harmonic force field were used for estimation of starting geometry and vibrational amplitudes in Least Square (LS) structural analysis of gas electron diffraction (GED) intensities.

Vibrational corrections to internuclear distances $\Delta r = r_{h1} - r_a$, necessary for geometric constructions during LS analysis, were calculated in the harmonic approximation using the VibModule program[38] taking into account the non-linear interrelation between internal and Cartesian vibrational coordinates according to Sipachev's theory.[39]

To visualize the results of QC and the results of LS analysis of GED data, the ChemCraft program was used.[40] NBO[36] calculations were used to investigate the likely conjugation of the carbon skeleton of the phenyl rings with the porphyrin moiety. The NCI[41] method was used to identify and visualize "weak" interactions in H_2TPP by open-source Multiwfn software.[42,43] These interactions (Figure S2) were quantitatively evaluated using the FI-SAPT0 method[44-46] implemented in the PSI4 program.[43] The aug-cc-pVTZ basis set was used in FI-SAPT0 calculations.

Syntheses

5,10,15,20-Tetraphenylporphyrin, H_2TPP. The synthesis was carried out according to a procedure based on the recommendations outlined in [47]. 4.0 mL of trifluoroacetic acid and 300.0 mL of para-xylene were placed into a 1 liter three-necked flask equipped with a Dean-Stark trap, reflux condenser, gas inlet, and dropping funnel. 14.3 mL (0.14 mol) of benzaldehyde, 10.0 mL (0.14 mol) of pyrrole and 300.0 mL of para-xylene were placed in an dropping funnel. The flask was heated until para-xylene began to boil, a current of air was turned on, and the solution from the dropping funnel was added to the flask. After adding all the solution from the dropping funnel, the reaction mass continued to be heated with air purge for an hour. Next, the flask was cooled to room temperature, diethanolamine (4.0 mL) was added and the mixture was left overnight. The precipitated porphyrin was filtered off and washed with ethanol. The residue was dissolved in dichloromethane and chromatographed on Brockmann grade II alumina, eluting with dichloromethane. The porphyrin eluate was evaporated and precipitated with ethanol. Yield: 8.1 g (38 %). ^{1}H NMR ($CDCl_3$, 500 MHz) δ ppm: 8.90 s (8H, *β*-H), 8.24 – 8.29m (8H, 2,6-H-Ph), 7.76 – 7.84 m (12H, 3,4,5-H-Ph), -2.72 bs (2H, NH). UV-Vis ($CHCl_3$) λ_{max} nm (lgε): 647(3.82), 590(3.86), 550(4.03), 515(4.27), 418(5.67). MALDI-TOF MS *m/z:* calculated: $C_{44}H_{30}N_4$, 614.25; found: 614.23.

Knudsen effusion experiment for obtaining sublimation enthalpy

Mass spectra of H_2TPP vapor were recorded and the Knudsen effusion experiment was carried out by a mass spectrometer MI 1201 with magnetic mass analyzer. A H_2TPP sample was sublimated from a molybdenum effusion cell. The ratio of the cell's internal cross-sectional area to the effusion orifice's area was about 1000. To measure the cell temperature, a W-Re 5/20 tungsten-rhenium thermocouple was used. The ionizing voltage was equal 45 V. The evaporator and ionization chamber parts had autonomous vacuum pumping using two turbomolecular pumps. The residual pressure in the evaporator was $5 \cdot 10^{-5}$, and in the ionization chamber $3 \cdot 10^{-6}$ Pa. The dependence of parent ion current vs. temperature of effusion cell in Arrhenius coordinates is shown in Figure 2. The presented graph is an overlay of points obtained both when the temperature increases from the lower to the upper, and when it decreases from the upper to the lower. The points form a single linear dependence, there is no hysteresis, and this circumstance indicates the achievement of thermodynamic equilibrium, as well as the low dependence of the heat capacity of H_2TPP on temperature in this narrow temperature range.

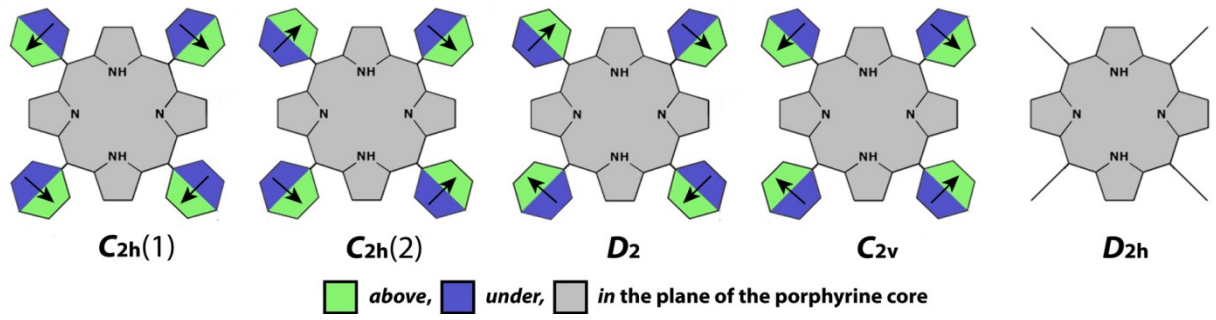

Figure 1. Considered conformations of H_2TPP.

Combined gas-phase electron diffraction/mass spectrometric experiment and structural analysis

In order to ensure the absence of thermal decomposition of the sample and volatile impurities, the diffraction pattern was recorded while simultaneously continuously monitoring the mass spectrum of vapors entering the ionization chamber of the mass spectrometer from the scattering volume of the electron diffraction device. For this purpose, a combined EMR-100/APDM-1 unit[48-50] was used. A sample of H_2TPP was evaporated at 657(5) K from a molybdenum effusion cell with a cylindrical effusion nozzle of 0.5 / 1.6 mm size (diameter / length). Diffraction patterns were registered on the MACO ES-209 Image Films at two nozzle-to-film distances 338 and 598 mm. Accurate wavelengths of electrons were determined using the polycrystalline zinc oxide standard. The main conditions of the GED/MS experiment are shown in Table S2. Digitization of films with diffraction patterns was carried out by modified computer-controlled microdensitometer MD-100 (Carl Zeiss, Jena).[51]

The most intense ions in the mass spectrum of H_2TPP recorded by MI 1201 during thermodynamic experiment and by EMR-100/APDM-1 during combined GED/MS experiment are given in Table 1.

Table 1. The most intensive ions in the mass spectrum of H_2TPP recorded by MI 1201 during thermodynamic experiment and by EMR-100/APDM-1 during combined GED/MS experiment.

Ion	*m/z*	I_{rel}[a]		
		MI 1201	EMR-100/APDM-1	
			L_1[b]=338 mm	L_2[b]=598 mm
$[C_{44}H_{30}N_4]^+$ $[M]^+$	614	100	100	100
$[C_{38}H_{25}N_4]^+$ $[M\text{-}Ph]^+$	537	8	11	5
$[C_{44}H_{30}N_4]^{++}$ $[M]^{++}$	307	10	23	19
U_{ioniz}, V		45	50	50
T, K		554	657	657

[a] ion intensity calculated relative to parent ion $[C_{44}H_{30}N_4]^+$;
[b] nozzle-to-film distance.

Three intensive ions were registered in the mass spectrum (*m/z*): the parent ion $[M]^+$ 614, the $[M\text{-}Ph]^+$ ion 537, and the doubly charged ion $[M]^{++}$ 307. The parent ion $[M]^+$ had the highest intensity in the mass-spectrum. The stoichiometric composition of the ions corresponds to the presence of a single molecular form of H_2TPP in the vapor under the experimental conditions.

Interpretation of electron diffraction intensities in terms of molecular structure within the framework of the least squares procedure was performed using the UNEX program.[52] MOCED[53] approach was used to reduce the number of varied structural parameters by fixing theoretical differences between some of them. The following parameters were used to describe the structure of H_2TPP (atom labeling is shown in Figure 3): twenty-four interatomic distances C_m-X_1, C_m-C_{a1}, C_m-C_{a2}, N_1-C_{a1}, N_2-C_{a2}, C_{a1}-C_{b1}, C_{a2}-C_{b2}, C_{b1}-X_3, C_{b2}-X_4, C_m-C_1, C_1-C_2, C_2-C_3, C_3-C_4, C_1-$C_{2'}$, $C_{2'}$-$C_{3'}$, $C_{3'}$-C_4, N_2-H, C_{b1}-H, C_{b2}-H, C_2-H, C_3-H, C_4-H, $C_{2'}$-H, $C_{3'}$-H; seventeen bond angles C_{a1}-C_m-X_1; C_{a2}-C_m-X_1; X_1-N_1-X_3; X_1-N_2-X_4; C_1-C_m-C_{a1}; C_2-C_1-C_m; $C_{2'}$-C_1-C_2; C_3-C_2-C_1; $C_{3'}$-$C_{2'}$-C_1; N_2-H-X_1; C_{a1}-C_{b1}-H; C_{a2}-C_{b2}-H; C_1-C_2-H; C_1-$C_{2'}$-H; C_2-C_3-H; $C_{2'}$-$C_{3'}$-H; C_3-C_4-H; twenty-one dihedral angles C_m-X_1-X_2-C_m; C_{a1}-C_m-X_1-X_2; C_{a2}-C_m-X_1-X_2; N_1-C_{a1}-C_{a1}-X_1; N_2-C_{a2}-C_{a2}-X_1; C_{b1}-X_3-C_{a1}-N_1; C_{b2}-X_4-C_{a2}-N_2; C_1-C_m-C_{a2}-N_2; C_2-C_1-C_m-C_{a2}; $C_{2'}$-C_1-C_2-C_m; C_3-C_2-C_1-$C_{2'}$; $C_{3'}$-$C_{2'}$-C_1-C_2; C_4-C_3-$C_{3'}$-$C_{2'}$; H-N_2-X_1-X_2; H-C_{b1}-C_{b1}-C_{a1}; H-C_{b2}-C_{b2}-C_{a2}; H-C_2-C_1-C_3; H-$C_{2'}$-C_1-$C_{3'}$; H-C_3-C_2-C_4; H-$C_{3'}$-$C_{2'}$-C_4; H-C_4-C_3-$C_{3'}$. The vibrational amplitudes were refined in groups in accordance with belonging to them internuclear distances to certain peaks on radial distribution function; eleven groups of amplitudes were formed (see Table S3).

The parameters to be refined in the LS analysis are given in Table 2. They were combined into 12 independent groups. Several variants of starting models based on the force fields from B3LYP and B97D were used in this work, and four models of conformers were tested. The results of LS analyses of GED intensities with force fields from QC calculations are given below.

Table 2. Scheme of independent refinement of molecular parameters in LS analysis of GED data.

Bond length	1)[a] C_m-C_{a1}, C_m-C_{a2}, N_1-C_{a1}, N_2-C_{a2}, C_{a1}-C_{b1}, C_{a2}-C_2, C_{b1}-X_3, C_{b2}-X_4, C_1-C_2, C_2-C_3, C_3-C_4, C_1-$C_{2'}$, $C_{2'}$-$C_{3'}$, $C_{3'}$-C_4, C -C_1 2) C_m-X_1 3) N_2-H, C_{b1}-H, C_{b2}-H, C_2-H, C_3-H, C_4-H, $C_{2'}$-H, $C_{3'}$-H
Bond angles	4) C_{a1}-C_m-X_1; C_{a2}-C_m-X_1 5) C_1-C_m-C_{a1} 6) C_2-C_1-C_m 7) $C_{2'}$-C_1-C_2; C_3-C_2-C_1; $C_{3'}$-$C_{2'}$-C_1
Torsion angles	8) C_2-C_1-C_m-C_{a2} 9) C_{a1}-C_m-X_1-X_2; C_{a2}-C_m-X_1-X_2 10) N_1-C_{a1}-C_{a1}-X_1; N_2-C_{a2}-C_{a2}-X_1 11) C_{b1}-X_3-C_{a1}-N_1; C_{b2}-X_4-C_{a2}-N2 12) $C_{2'}$-C_1-C_2-C_m; C_3-C_2-C_1-C_m; $C_{3'}$-$C_{2'}$-C_1-C_m; C_4-C_3-$C_{3'}$-C_2

[a] Label of parameters group. The difference between parameters of the same group is fixed at the QC values.

Results and Discussion

Knudsen effusion experiment results

The conditions and details of the Knudsen experiment with mass spectrometric monitoring the vapor composition are given in Experimental part.

The enthalpy of sublimation was determined within the framework of the II law of thermodynamics. Determining enthalpies using this approach does not require vapor pressure calibration of the instrument, and the errors associated with the estimation of ionization cross-sections are removed. In this case, to determine the heat of sublimation one can use not the equilibrium constants K themselves, but the values K_{IT}, proportional to the constants, which are expressed through ionic currents and do not include ionization cross sections. The measured temperature dependence of the ln(IT) = f(1/T) is shown in Figure 2.

Based on the slope tangent of this dependence, the reaction enthalpy is calculated using the least-squares method based on the Clausius-Clapeyron equation:

$$\frac{d\ln K_I}{dT} = -\frac{\Delta_{sub} H^{o}_{m}(T)}{RT}$$

The heat of sublimation of the H_2TPP was obtained equal to 212(4) kJ/mol at 535K. This value differs sharply from the values obtained in [22,23,26,27] using gas-phase absorption spectra, fluorescence of molecular beams, and the Knudsen effusion method without mass spectrometric control. At the same time, the average value of 214 kJ/mol, calculated on the basis of values obtained by inert gas transfer methods[24,25] and Knudsen effusion mass spectrometry,[20] is in excellent agreement with our result, which indicates its reliability and allows recommend a value of 212(4) kJ/mol at 535 K as the value of the heat of sublimation of the H_2TPP.

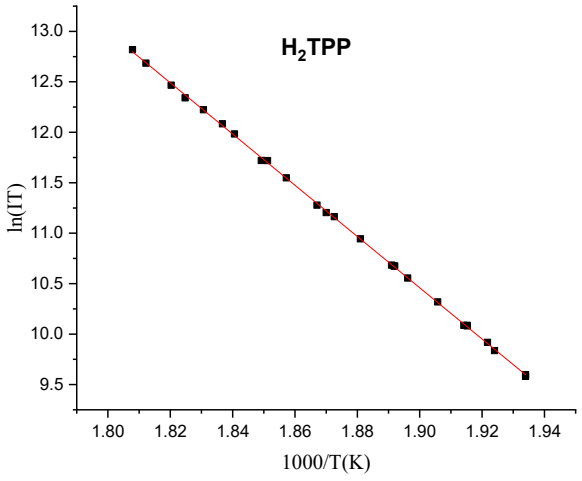

Figure 2. Temperature dependence of the molecular ion intensity logarithm in the range 510-564 K.

Conformational properties of the H_2TPP molecule according to calculations

As noted in the Introduction, at first glance, due to the steric repulsion of phenyl fragments from the MHC skeleton, the free H_2TPP molecule should have D_{2h} symmetry (Figure 1) and not have other conformers associated with different orientations of the four phenyl substituents relative to each other and the skeleton of the molecule.

However, X-ray diffraction data show that the molecules in the crystal have a structure whose symmetry is close to C_{2h}(1). This circumstance indicates the need to consider other possible conformers with a sloped position of phenyl substituents relative to the MHC skeleton (Figure 1).

Figure 1 shows possible conformations that have a second-order symmetry axis. For each structure, a complete optimization of the geometry and calculation of vibration frequencies was performed with two functionals of DFT method, B97D and B3LYP.

Both the inclusion and exclusion of the dispersion correction in the DFT functional give a qualitatively similar conformational composition of H_2TPP. Four stable conformers were found with close relative energies. The difference between them is less than 0.22 kcal/mol in calculations using the B3LYP functional and less than 0.84 kcal/mol with the B97D functional (Table 3). The C_{2v} symmetry conformer corresponds to the global minimum on the potential energy surface (PES).

In the case of the D_{2h} conformation, there are four imaginary frequencies corresponding to the torsional motions of the C_6H_5 fragments. Thus, it can be assumed that the sloped position of the phenyl meso-substituents is a structural feature of both metal-free tetraphenylporphyrin and its complexes with metals,[19] but the balance of forces leading to such equilibrium configuration remains unclear.

Table 3. Relative energies of H_2TPP conformers, torsion angles and disagreement factor values R_f[1] by calculations, (ΔE kcal/mol, θ deg).

	C_{2v}	C_{2h}(1)	C_{2h}(2)	D_2	D_{2h}
B3LYP/cc-pVTZ					
ΔE	0.00	0.05	0.12	0.22	0.26 (SP4)[3]
θ (C_2-C_1-C_m-C_{a2})[2]	72.6	74.5	75.3	79.8	90.0
B97D/cc-pVTZ					
ΔE	0.0	0.31	0.43	0.84	2.41 (SP4)
θ (C_2-C_1-C_m-C_{a2})	61.5	64.6	64.4	67.0	90.0
R_f, %	0	2.2	2.3	3.5	8.6

[1]Disagreement factor between the theoretical functions of the molecular scattering intensity, calculated with respect to the conformer of C_{2v} symmetry.
[2]For atom labeling see Figure 3.
[3]SP4 is a saddle point of the fourth order.

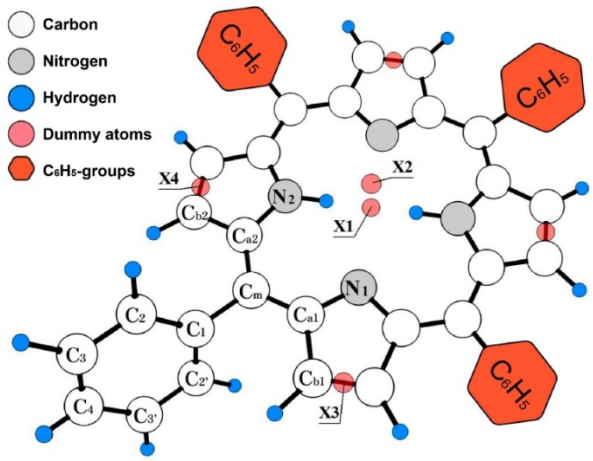

Figure 3. Atom labeling in the structure of H_2TPP.

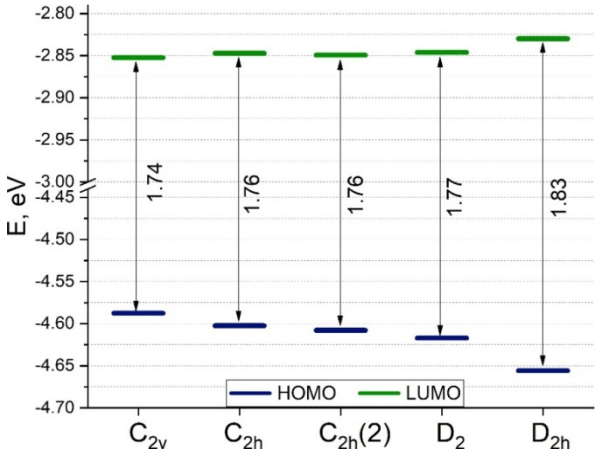

Figure 4. Energies of frontier orbitals in H_2TPP conformers (B97D/cc-pVTZ).

The difference in bond lengths of conformers within the same level of the QC is insignificant, 0.001 Å (Tables S4, S5). However, there is a noticeable difference in the values of the torsion angle θ with different relative orientations of the four phenyl substituents. In Table S5 the dihedral angles characterizing the out-of-plane distortions of the MHC skeleton are given for all conformers. A smaller angle θ corresponds to a more distorted core of the conformer. It should be noted that the degree of non-planar deformation of the MHC is reflected in the energy of the frontier orbitals of the H_2TPP conformers and affects the reactivity of the compound.[29] The greater the out-of-flatness of the MHC, the smaller the difference between the HOMO and LUMO energies (Figure 4).

The question of choosing the electron density functional deserves special attention, since the structural parameters predicted in calculations with different functionals can differ markedly.

A comparison of the calculated geometric parameters for the equilibrium configuration of the $C_{2h}(1)$ symmetry conformer with the experimental parameters of the molecule in the crystal (Table S1, angle θ ~60°) showed that the use of the B97D functional leads to their better agreement compared to the B3LYP functional (Table 4). Therefore, the results based on calculations DFT/B97D/cc-pVTZ theoretical level are presented in text, and the similar results obtained by the DFT/B3LYP/cc-pVTZ method are given in SI. Note that the difference for the same conformer bond lengths, calculated with different functionals, reaches 0.006 Å (Table S3), which exceeds the error in their determination in the GED experiment. This discrepancy indicates the importance of choosing an appropriate level of theory for calculating the molecular structure of this class of compounds and makes it relevant to study this compound by GED/MS method.

The diagram of transitions between conformers indicating the structure of transition states and values of barriers is presented in Figure 5. As can be seen, the energy required for most conformational transitions does not exceed 1.3 kcal/mol.

This conclusion is of fundamental importance for the interpretation of GED data, since it allows to compare the thermal energy RT = 1.3 kcal/mol under the conditions of the GED/MS experiment with the barriers to transitions between conformers.

To clarify the fundamental possibility to distinguish conformers using the GED method, calculations of theoretical curves of the radial distribution f(r) for each of conformer and the difference $\Delta f(r) = f(r)_{C2v} - f(r)_{i\ conf}$ were performed (Figures S4, S5).

It can be noted that the main differences in the $f(r)_i$ plots belong to the region > 2 Å. They refer to the intermolecular distances between unbounded atoms of *meso*-substituents and the atoms of the porphyrin macrocycle that define the value of the dihedral angle $\theta(C_2\text{-}C_1\text{-}C_m\text{-}C_{a2})$.

The R_f values and difference curves in Figures S4, S5 show that it is in principle possible to determine the symmetry of a conformer if the gas phase contains a single conformer.

To estimate the errors in determining the angle $\theta(C_2\text{-}C_1\text{-}C_m\text{-}C_{a2})$ and dihedral angles characterizing the non-planarity of the MHC by GED method, the potential energy surface U(θ) was scanned along the coordinate θ (Figure 6a) for one of the conformers (C_{2v}) .

The function U(θ) was obtained with fixing a values of θ and refining all other geometric parameters.

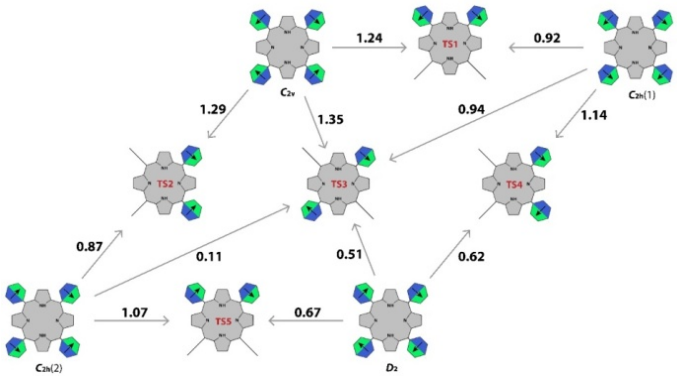

Figure 5. Scheme of transitions between H_2TPP conformers and transition barriers (in kcal/mol; B97D).

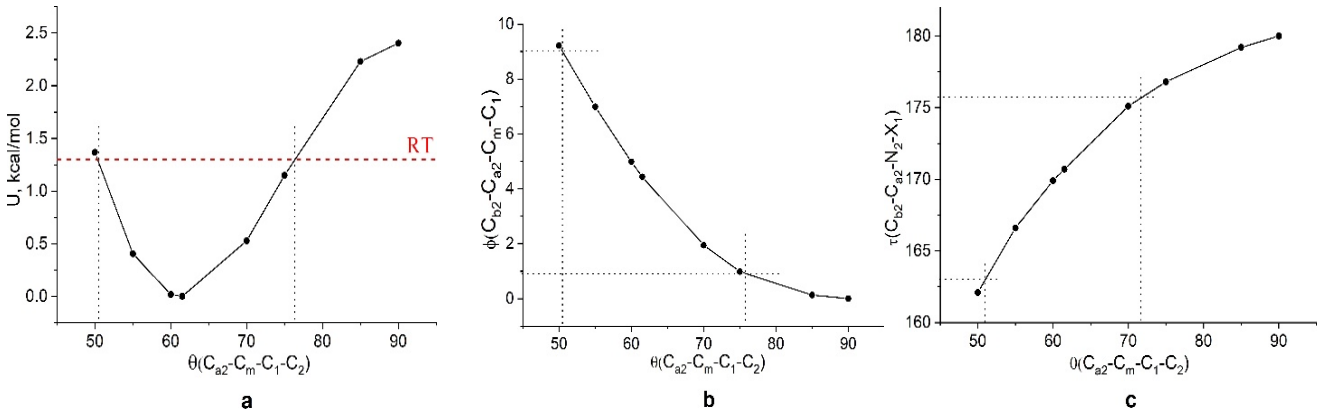

Figure 6. a) The dependence of the relative energy of the conformer on the torsion angle θ(C2-C1-Cm-Ca2); b) and c) the dependences of the angles ϕ and τ, which determine the tilt of the pyrrole fragment in the MHC on the value of the angle θ.

The functions ϕ=*f*(θ) and τ=*f*(θ) (Figure 6b,c) reflect the relationship between the ϕ and τ angles of non-planar distortion of the macrocyclic skeleton from the torsion angle θ.

Figure 6 shows that the thermal energy RT (dashed line) corresponds to a change in the torsion angle θ in the range of 51–72°, and the angles ϕ and τ – in the range of 9–1° and 163–176°, respectively.

Results of structural analysis of gas-phase electron diffraction data

The calculated geometric parameters of the four conformers of the H_2TPP molecule (Tables S4, S5) were used as starting values, which were then refined in least squares analysis (LS) of the GED data (details of the structural analysis technique are given in Experimental).

Figure 7 shows the experimental radial distribution function and its theoretical analog obtained with the starting values of the structural parameters of the C_{2v} model, as well as the difference functions $\Delta f(r) = f_{exp}(r) - f_{theor}(r)$ corresponding to the starting models of other conformers. It can be seen that, regardless of the starting model, after optimization all difference curves practically do not differ from each other, as well as the values of the disagreement factor R_f, and this one testifies to stability of solution of optimisation task.

Tables 4 and 5 show the optimized geometric parameters of conformers obtained from experimental GED data for different starting models. The optimized structural parameters for different starting models coincide within the error of their determination, which, in particular, indicates the stability of the optimization task.

It was noted above, that the GED method could distinguish individual conformers, since the difference in R_f between their theoretical functions *f*(r) was more than 2% (Figure S4).

The result obtained (Figure 7, Tables 4 and 5) can be explained if to suppose that in saturated vapor at T = 657 K there is a mixture of H_2TPP conformers. Moreover, at the experimental temperature, conformers, as shown by TS calculations (Figure 5), can transform into each other.

Solving the structural problem for a given mixture of conformers by GED seems difficult due to the large number and closeness of corresponding structural parameters of conformers (more than 1000 terms for each).

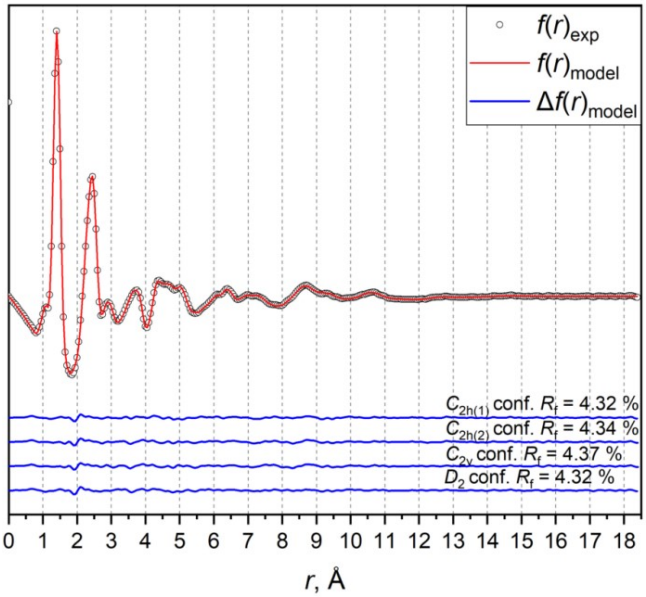

Figure 7. Experimental radial distribution function and its theoretical analog obtained with starting values of the structural parameters of the C_{2v} model, as well as difference functions Δf(r) corresponding to theoretical models of other conformers of H_2TPP molecule.

Nevertheless, despite the complexity of GED data interpretation and a certain ambiguity in the structural parameters of gaseous H_2TPP, several confident conclusions can be made:

(i) all bond lengths of the porphyrin skeleton and phenyl substituents, which are almost identical in all conformers, were determined with high accuracy (Table 4);

(ii) calculations using the B97D functional more accurately predict bond lengths and bond angles in H_2TPP molecules than calculations using the B3LYP functional (Table 4);

(iii) the position of the phenyl substituents relative to the MHC skeleton differs from orthogonal, the torsion angle θ is determined within the range of 65-81°.

Table 4. Experimental r_{h1} and calculated r_e bond lengths and bond angles of H_2TPP (Å, deg.)

Method	r_{h1} GED				r_e QC		X-Ray[9-16]	
Starting model	C_{2v}	$C_{2h}(1)$	$C_{2h}(2)$	D_2	C_{2v} B97D	C_{2v} B3LYP	min	max
R_f, %, GED	4.37%	4.32%	4.34%	4.32%	-	-	-	-
N_1-C_{a1}	1.369(3)	1.369(3)	1.370(3)	1.370(3)	1.367	1.362	1.359	1.374
N_2-C_{a2}	1.379(3)	1.379(3)	1.379(3)	1.379(3)	1.376	1.372	1.366	1.378
C_{a1}-C_{b1}	1.462(3)	1.462(3)	1.462(3)	1.462(3)	1.459	1.456	1.427	1.459
C_{a2}-C_{b2}	1.436(3)	1.436(3)	1.436(3)	1.436(3)	1.433	1.430	1.417	1.432
C_{b1}-C_{b1}	1.362(3)	1.362(3)	1.362(3)	1.362(3)	1.357	1.348	1.332	1.383
C_{b2}-C_{b2}	1.377(3)	1.376(3)	1.377(3)	1.377(3)	1.372	1.364	1.348	1.381
C_m-C_{a1}	1.416(3)	1.415(3)	1.415(3)	1.415(3)	1.413	1.406	1.392	1.408
C_m-C_{a2}	1.409(3)	1.409(3)	1.408(3)	1.408(3)	1.406	1.399	1.394	1.404
C_m-C_1	1.494(4)	1.495(4)	1.495(4)	1.496(4)	1.491	1.497	1.487	1.504
C_1-C_2	1.407(3)	1.407(3)	1.407(3)	1.406(3)	1.405	1.397	1.372	1.400
C_2-C_3	1.399(3)	1.399(3)	1.399(3)	1.400(3)	1.396	1.390	1.376	1.396
C_3-C_4	1.401(3)	1.401(3)	1.401(3)	1.401(3)	1.398	1.390	1.357	1.391
N-C_{a1}-C_{b1}	111.9(5)	112.0(5)	111.8(6)	111.9(5)	110.9	110.7	109.5	110.8
N-C_{a2}-C_{b2}	107.5(5)	107.7(5)	107.4(6)	107.6(5)	106.5	106.4	106.4	108.6
C_{a1}-C_{b1}-C_{b1}	105.9(2)	105.9(2)	105.9(2)	105.9(2)	106.3	106.4	106.3	107.1
C_{a2}-C_{b2}-C_{b2}	107.8(2)	107.7(2)	107.8(2)	107.7(2)	108.1	108.2	107.2	108.5
C_{a1}-N-C_{a1}	104.4(7)	104.2(7)	104.4(7)	104.4(6)	105.6	105.8	105.0	109.9
C_{a2}-N-C_{a2}	109.6(7)	109.2(7)	109.6(7)	109.4(7)	110.7	110.8	105.2	110.2
C_{a1}-C_m-C_{a2}	127.0(10)	126.9(10)	126.1(9)	125.6(1)	125.4	125.3	124.8	125.6

Table 5. Distances between non-bonded atoms of the coordination cavity and torsion angles obtained using different starting models

Method	GED T=657 K				X-Ray[1-8]	
Starting model	C_{2v}	$C_{2h}(1)$	$C_{2h}(2)$	D_2	min	max
R_f%	4.37%	4.32%	4.34%	4.32%		
N_1...X_1	2.042(12)	2.037(10)	2.044(18)	2.026(7)	2.015	2.041
N_2...X_1	2.109(11)	2.102(11)	2.097(9)	2.093(8)	2.088	2.119
C_m...C_m	6.912(20)	6.909(18)	6.912(21)	6.921(34)	6.861	6.938
N_1…N_1	4.085(23)	4.073(20)	4.088(36)	4.052(14)	4.031	4.230
N_2…N_2	4.218(21)	4.205(22)	4.195(18)	4.185(15)	4.042	4.237
C_2-C_1-C_m-C_{a2}	72.5(117)	73.0(78)	74.8(59)	77.4(47)	57.7	62.6
C_{b1}-C_{b1}-C_{a1}-N_1	4.9(56)	5.4(111)	7.1(119)	5.1(94)	0.0	1.5
C_{b2}-C_{b2}- $C_{\alpha2}$-N_2	4.9(51)	1.5(156)	6.7(110)	5.0(91)	0.1	1.3
C_{a1}-N_1-N_1-C_{a1}	164.6(116)	179.8(233)	179.7(274)	179(224)	180.0	180.0
C_{a2}-N_2-N_2-$C_{\alpha2}$	167.0(74)	179.8(210)	179.8(264)	180(205)	180.0	180.0
C_{a1}-N_1-N_2-C_{a2}	10.7(51)	2.8(72)	5.1(65)	0.4(36)	2.4	4.6
C_{b1}-C_{a1}-N_1-X_1	172.8(38)	178(41)	174.4(40)	178.1(35)	177.4	178.7
C_{b2}-C_{a2}-N_2-X_1	173.9(38)	172.1(41)	177.5(41)	178.1(34)	165.5	167.2

(B97D) in the GED experiment, and X-ray parameters of H_2TPP (Å, deg.).

Features of geometric and electronic structure of H_2TPP - From H_2P to H_2TPP and from H_2TPP to MTPP

The introduction of a certain substituent along the periphery of the macrocycle or the introduction of a metal atom into the coordination cavity makes it possible to specifically modify the physicochemical properties of the resulting compounds.

The change in the characteristics of the electronic and geometric structure of unsubstituted porphyrin (H_2P) with the introduction of a bulky *meso*-substituent C_6H_5 or C_6H_4F, as well as with the transition from H_2TPP to complexes of tetraphenylporphine with zinc and palladium (Table 6), is considered in this section.

As noted in [18,19], the energy balance of donor-acceptor (*d-a*) interaction ($E_{d\text{-}a}$) and steric repulsion (E_{ster}) between phenyl fragments and macrocycle skeleton is a possible reason for the non-orthogonal position of phenyl substituents relative to MHC core in H_2TFPP, ZnTPP and PdTPP molecules.

To test this hypothesis, the change in energy $E_{d\text{-}a}$ with a change in the torsion angle $\theta(C_2\text{-}C_1\text{-}C_m\text{-}C_{a2})$ in the range of 50–90° was considered (Figure 8) within the framework of NBO analysis.[36] The energy $\Sigma E_{d\text{-}a}$, which stabilizes a certain geometry, decreases sharply with increasing θ from 50 to 75°, and changes slightly in the range θ=75–90°.

Interactions of the type $\pi(C_{a1}\text{-}C_m) \rightarrow \pi^*(C_1\text{-}C_2)$ (5 kcal/mol) give the largest contribution to $\Sigma E_{d\text{-}a}$ at θ=50°, and at θ=75° interactions of the type $\pi(C_{a1}\text{-}C_m) \rightarrow \sigma^*(C_1\text{-}C_2)$ (2 kcal/mol) dominate (Figure 8). Thus conjugation of the carbon skeleton of the phenyl rings with the porphyrin moiety weakens with increasing angle θ.

In addition to the *d-a* interaction, we estimated the energy of steric repulsion between the phenyl fragments and the MHC skeleton within the framework of a limited model including pyrryl, pyrrole and phenyl fragments (Figure S6).

In this case, both the FI-SAPT0 approach described in [44-46], and the assessment of steric interaction between different fragments of the molecule by NBO method[36] were used. Both approaches reflect the same tendency for the steric repulsion to decrease with increasing angle θ (Figure S2).

A decrease in E_{ster} as the angle θ increases and an increase in $\Sigma E_{d\text{-}a}$ as θ decreases lead to a slope position of the phenyl substituents in H_2TPP.

The value of the angle θ, different from 90° and obtained in calculations for conformers, corresponds to the optimal relationship between the energies of *d-a* interaction and steric repulsion.

Note that in all compounds (Table 6) the values of the angle $\theta(C_2\text{-}C_1\text{-}C_m\text{-}C_{a2})$, determined in the GED, are greater than its calculated value. This may be a consequence of the complex conformational composition of the vapor, as well as underestimated harmonic vibrational corrections to internuclear distances due to the flexibility of the MHC and large amplitudes of torsional vibrations of phenyl substituents.

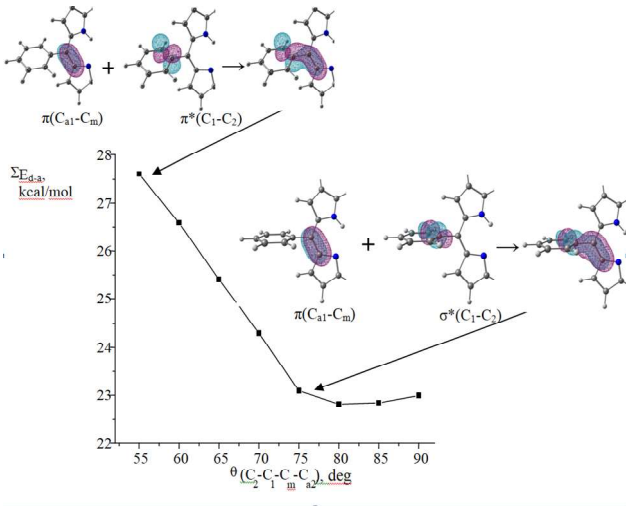

Figure 8. Dependence of the $\Sigma E_{d\text{-}a}$ between the NBO of the phenyl fragment and the orbitals of the MHC skeleton on the torsion angle $\theta(C_2\text{-}C_1\text{-}C_m\text{-}C_{a2})$.

The influence of phenyl meso-substituents on the geometric and electronic characteristics of porphyrins

The introduction of a bulky C_6H_5 substituent into the meso-position leads to changes in the geometry of the macroheterocyclic skeleton, which is expressed not only in its non-planar deformation, but also in a change in the lengths of the $C_m\text{-}C_{a1}$ and $C_m\text{-}C_{a2}$ bonds, as well as the $C_{a1}\text{-}C_m\text{-}C_{a2}$ bond angle between them. These bonds are lengthened by 0.012 Å, and the bond angle is reduced by ~ 2°. Such changes in the geometry of the core are characteristic of the donor nature of the substituents and are explained by the theory of valence shell electron pair repulsion (VSEPR).[54] According to this theory, the donor substituent, in our case phenyl, increases the electron density on the hybrid orbital $h(C_m \rightarrow C_1)$ of the C_m atom, which overlaps with the hybrid orbital of the C_1 atom of the phenyl substituent. The volume of this orbital increases, which is reflected in an increase in the contribution of the s-orbital, a decrease in the contribution from p-AO and a change in the type of hybridization from $sp^{2.72}$ in H_2P to $sp^{2.22}$ in H_2TPP (Table 6). As a result, the type of hybridization changes in the other two orbitals of the C_m atom, $h(C_m \rightarrow C_{a1})$ and $h(C_m \rightarrow C_{a2})$, in which the contribution of p-AO increases. The latter leads to an elongation of the $C_m\text{-}C_{a1}$ and $C_m\text{-}C_{a2}$ bonds and a decrease in the repulsion between the electron densities of these bonds and a decrease in the $C_{a1}\text{-}C_m\text{-}C_{a2}$ bond angle in H_2TPP compared to H_2P (Table 6). The transition from H_2TPP to H_2TFPP does not lead to a change in the characteristics of the core, and the changes upon transition to the ZnTPP complex are due to an increase in its symmetry.

Figure 9 shows a diagram of the energies of the frontier orbitals for the molecules H_2P, H_2TPP, H_2TFPP, ZnTPP and PdTPP. The introduction of electron-donating phenyl substituents leads to an increase in the HOMO energy (from H_2P to H_2TPP).

Table 6. Selected characteristics of the electronic and geometric structure of H_2P, H_2TPP, H_2TFPP, ZnTPP and PdTPP molecules.

Parameters[1]	H_2P	H_2TPP	H_2 TFPP	ZnTPP	PdTPP
E_{HOMO}, eV	-4.86	-4.59	-4.77	-4.63	-4.75
E_{LUMO}, eV	-2.90	-2.85	-3.05	-2.80	-2.76
$\Delta E_{LUMO-HOMO}$, eV	1.96	1.74	1.72	1.83	1.99
r(C_m-C_{a1}), Å	1.401	1.413	1.414	1.409	1.401
r(C_m-C_{a2}), Å	1.395	1.406	1.407	1.409	1.401
r(C_m-C_1), Å	-	1.492	1.490	1.492	1.492
α(C_{a1}-C_m-C_{a2}), °	127.2	125.4	125.3	125.2	124.4
h(C_m-C_1)	$sp^{2.72}$	$sp^{2.22}$	$sp^{2.21}$	$sp^{2.23}$	$sp^{2.20}$
h(C_m-C_{a1})	$sp^{1.68}$	$sp^{1.83}$	$sp^{1.84}$	$sp^{1.90}$	$sp^{1.91}$
h(C_m-C_{a2})	$sp^{1.78}$	$sp^{1.97}$	$sp^{1.96}$	$sp^{1.90}$	$sp^{1.91}$
θ(C_2-C_1-C_m-C_{a2}),° QC	-	61.5	60.3	62.7	64
θ(C_2-C_1-C_m-C_{a2}),° GED	-	73(8)	$82(^{-24+50})$[18]	80.3(36)[19]	83.3(175) [19]
Z(TPP), e		-0.912	-0.918	-1.196	-0.529

[1] The values calculated in this work by the B97D/cc-pVTZ method are presented; the type of AO hybridization and the charge *Z(TPP)* on the TPP fragment were obtained within the framework of NBO analysis.

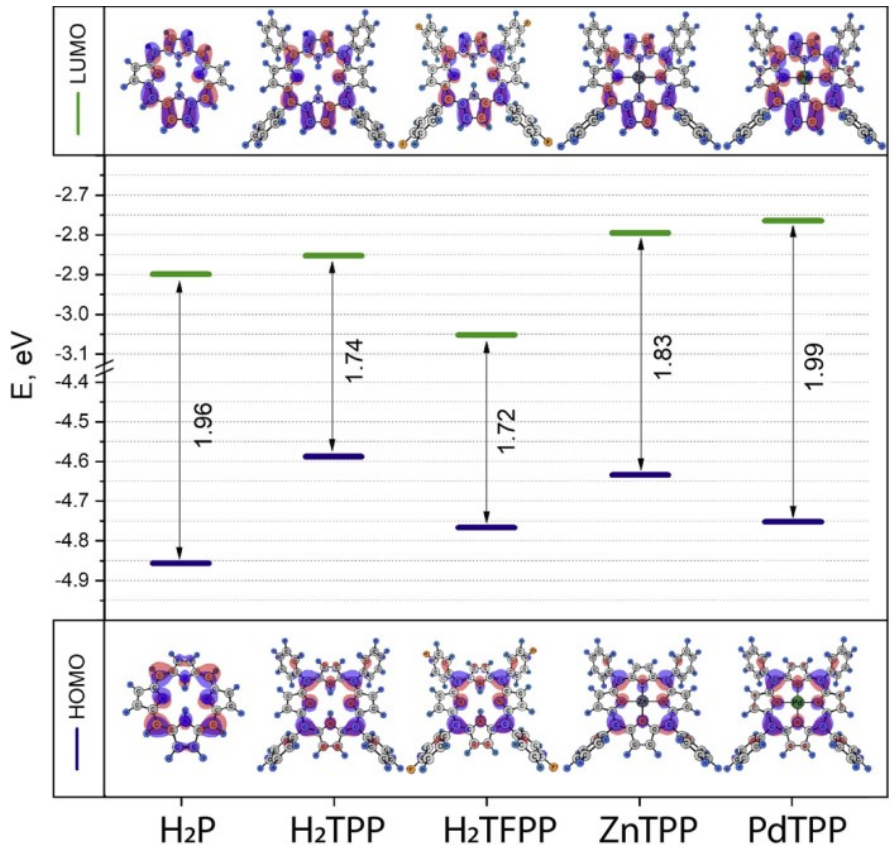

Figure 9. Energy diagram of frontier orbitals for molecules H_2P, H_2TPP, H_2FTPP, ZnTPP and PdTPP (for ZnTPP and PdTPP one of the two degenerated LUMOs is shown).

The HOMOs of all molecules are π-MOs, the main contribution to which is made by pπ-AOs included in the internal perimeter of the MHC skeleton. Moreover, the AO of phenyl fragments makes an insignificant contribution to the HOMO of H_2TPP, H_2TFPP, ZnTPP and PdTPP.

Fluorination of phenyl substituents (transition from H_2TPP to H_2TFPP) leads to a decrease in the energies of the frontier orbitals, which is determined by the electron-withdrawing nature of fluorine atoms and a significant redistribution of electron density in the carbon sceletone of the phenyl substituents.

The similarity of the energies of the frontier orbitals, the C_m-C_{a1} and C_m-C_{a2} bond lengths, as well as the C_{a1}-C_m-C_{a2} bond angle in H_2TPP and ZnTPP may be a consequence of the similar values of the electronic charge *Z(TPP)* distributed over the TPP fragment in H_2TPP and ZnTPP.

When going from ZnTPP to PdTPP, the charge on the TPP fragment decreases significantly, *i.e.* Pd atom, compared to Zn atom, is more electron-withdrawing, which reduces the electron-donating effect from phenyl substituents. This results in a lower HOMO energy in the PdTPP complex relative to the HOMO in ZnTPP.

An additional reason for the increase in the energy gap between the HOMO and LUMO during the transition from H_2TPP to ZnTPP and PdTPP is the decrease in the out-of-plane distortion of the macroheterocyclic core, which is associated with an increase in the torsion angle θ(C_2-C_1-C_m-C_{a2}). The metal atom in the coordination cavity of the MHC makes it more rigid, which leads to a smaller deviation of the phenyl fragments from the perpendicular position (Table 4).

The frontier orbital diagram shows in which direction the red-ox properties of compounds will change with various modifications of porphyrin compounds.

Conclusion

Using the Knudsen effusion mass spectrometry method, the heat of sublimation of the H_2TPP was determined to be 212(4) kJ/mol at 535 K, which made it possible to eliminate the contradictions in the literature. It has been shown that the H_2TPP compound is thermally stable up to at least 660 K and can be used in CVD technologies. The composition of ions in the mass spectrum does not change with increasing temperature; all ions have a single molecular precursor, H_2TPP.

Conformational analysis for the H_2TPP molecule was performed using the DFT method with the B97D and B3LYP functionals. Both methods showed that the molecule has four conformers in which the phenyl substituents occupy a sloping position relative to the MHC skeleton. Conformers differ in the mutual orientation of the substituents and the value of the torsion angle. The energy barriers between conformers are calculated and it is shown that the structure of D_{2h} symmetry is a fourth-order saddle point.

An electron diffraction study of saturated vapor was carried out at T = 657 K. It was shown that the complex conformational composition of the vapor corresponds to the experimental data, the values of bond lengths and bond angles were reliably determined, while the error in determining torsion angles and dihedral angles in MHC reaches 10°.

Within the framework of NBO, the energy of donor-acceptor interaction was calculated. It has been shown that at a torsion angle θ=50–70° there is a noticeable delocalization of the electron density between the phenyl fragments and the MHC skeleton, which contributes to a decrease in the total energy. The energy of donor-acceptor interaction $\Sigma E_{d\text{-}a}$ decreases significantly with increasing θ. The value of the angle θ, different from 90°, obtained in calculations for different conformers and in experiment, corresponds to the optimal relationship between the energies of donor-acceptor interaction and steric repulsion.

In the crystalline state, a structure is realized that is close to the structure of one of the conformers of the free molecule, which ensures close packing with the shortest distances of ~2.9 Å between the phenyl fragment of one molecule and the skeleton of the neighboring molecule.

It has been established that the H_2TPP molecule has conformational non-rigidity and can be considered as a reference compound when comparing the structural properties of compounds created by substitution in coordination cavity and periphery of macroheterocyclic skeleton. The change in geometric and electronic characteristics in the series of molecules H_2P, H_2TPP, H_2TFPP, ZnTPP and PdTPP is considered. Based on the VSEPR theory, an explanation is given for the influence of the substituent on the parameters of the MHC skeleton. Analysis of changes in the energy of frontier orbitals in the indicated series of molecules makes it possible to predict in which direction the red-ox properties of compounds will change with various modifications of porphyrin compounds.

Acknowledgements. This work was supported by the Russian Science Foundation (grant No 20-13-00359). The gas-phase electron diffraction/mass-spectrometric experiments were carried out using the GED/MS equipment (*https://www.isuct.ru/department/ckp/structure/ged-ms*) of the resources of the Centre for Shared Use of Scientific Equipment of the ISUCT (with the support of the Ministry of Science and Higher Education of Russia, grant No. 075-15-2021-671).

References

1. *Handbook of Porphyrin Science* (Kadish K.M., Smith K.M., Guilard R., Eds.), World Scientific: Singapore, **2010**, 6 – 10, ISBN 978-9814307185.
2. Li L.-L., Diau E. W.-G. *Chem. Soc. Rev.* **2013**, *42*, 291–304; doi: 10.1039/C2CS35257E.
3. Bonnett R. *Chem. Soc. Rev.* **1995**, *24*, 19; doi: 10.1039/cs9952400019.
4. Ding Y., Zhu W.-H, Xie Y. *Chem. Rev.* **2017**, *117*, 2203–2256; doi: 10.1021/acs.chemrev.6b00021.
5. Senge M. O., Fazekas M., Notaras E.G.A., Blau W.J. Zawadzka M., Locos O.B., Ni Mhuircheartaigh E.M. *Adv. Mater.* **2007**, *19*, 2737–2774, doi: 10.1002/adma.200601850.
6. Pukhovskaya S.G., Dao Tkhe Nam, Ivanova Yu.B., Liulkovich L.S., Semeikin A.S., Syrbu S.A., Kruk M.M. *J. Incl. Phenom. Macrocycl. Chem.* **2017**, *89*, 325–332, doi: 10.1007/s10847–017–0758–9.
7. Silva P., Vilela S.M.F., Tome J.P.S., Paz F.A. *Chem. Soc. Rev.* **2015**, *44*, 6774-6803, doi: 10.1039/c5cs00307e.
8. Hamor M.J., Hamor T.A., Hoard J.L. *J. Am. Chem. Soc.* **1964**, *86*, 1938–1942, doi: 10.1021/ja01064a008.

9. Silvers S.J., Tulinsky A. *J. Am. Chem. Soc.* **1967**, *89*, 3331–3337, doi: 10.1021/ja00989a036.
10. Kano K., Fukuda K., Wakami H., Nishiyabu R., Pasternack R.F. *J. Am. Chem. Soc.* **2000**, *122*, 7494–7502, doi: 10.1021/ja000738g.
11. Li Z., Hu Y., Li T. *Mol. Cryst. Liq. Cryst.* **2014**, *605*, 135–145, doi: 10.1080/15421406.2014.884403.
12. Andreev V., Sobolev P., Tafeenko V. TPHPOR16. *CSD Commun. (Private Communication)* **2018**, CCDC, 1554868.
13. Barker B.L., Stanley G.G., Fronczek R.F. TPHPOR11. *CSD Commun. (Private Communication)* **2002**, CCDC 188202.
14. Bruckner C., Ogikubo J., McCarthy J.R., Akhigbe J., Hylan, M.A., Daddario P., Worlinsky J.L., Zeller M., Engle J.T., Ziegler C.J., Ranaghan M.J., Sandberg M.N., Birge R.R. *J. Org. Chem.* **2012**, *77*, 6480–6494, doi: 10.1021/jo300963m.
15. Light M.E., Bandy T., Stulz E. TPHPOR13. *CSD Commun. (Private Communication)* **2016**, CCDC 1476315.
16. Han R., Kim S., Janda K.J., Fleischer E.B. *J. Porphyrins Phthalocyanines* **2018**, *22*, 355, doi: 10.1142/S1088424618500335.
17. Burmistrov V.A., Trifonova I.P., Islyaikin M.K., Semeikin A.S., Koifman, O.I. *ChemistrySelect* **2022**, *7*, e202103677, doi: 10.1002/slct.202103677.
18. Kurochkin I.Y., Pogonin A.E., Otlyotov A.A., Kiselev A.N., Krasnov A.V., Shlykov S.A., Girichev G.V. *J. Mol. Struct.* **2020**, *1221*, 128662, doi: 10.1016/j.molstruc.2020.128662.
19. Girichev G.V.: TverdovaN.V., Giricheva N.I., Savelyev D.S., Ol'shevskaya V.A., Ageeva T.A., Zaitsev A.V., Koifman O.I. *J. Mol. Struct.* **2019**, *1183*, 137–148, doi: 10.1016/j.molstruc.2019.01.055.
20. Kudin L.S., Dunaev A.M., Motalov V.B., Cavallo L., Minenkov Y. *J. Chem. Thermodyn.* **2020**, *151*, 106244, doi: 10.1016/j.jct.2020.106244.
21. Deachapunya S., Stefanov A., Berninger M., Ulbricht H., Reiger E., Doltsinis N. L., Arndt M. *J. Chem. Phys*. **2007**, *126*, 164304, doi: 10.1063/1.2721563.
22. Stefanov A., Stibor A., Dominguez-Clarimon A., Arndt M. *J. Chem. Phys.* **2004**, *121*, 6935- 6940, doi: 10.1063/1.1792551.
23. Torres L.A., Campos M., Enríquez E., Patico R. *J. Chem. Thermodyn*. **2002**, *34*, 293–302, doi: 10.1006/jcht.2001.0920.
24. Perlovich G.L., Golubchikov O.A., Klueva M.E. *J. Porphyrins Phthalocyanines* **2000**, *4*, 699–706, doi: 10.1002/1099–1409(200012)4:8<699::AID–JPP284>3.0.CO;2-M.
25. Golubchikov O., Perlovich G. In: *Advances in Chemistry of Porphyrins [Успехи химии порфиринов]* (Golubchikov O.A., Ed.), St. Petersburg, **1997**, Vol. *1*, p. 223–245.
26. Edwards L., Dolphin D.H., Gouterman M., Adler A.D. *J. Mol. Spectrosc.* **1971**, *38*, 16–32, doi: 10.1016/0022–2852(71)90090-7.
27. Bonderman D.P., Cater E.D., Bennett W.E. *J. Chem. Eng. Data* **1970**, *15*, 396–400, doi: 10.1021/je60046a004.
28. Tverdova N.V., Giricheva N.I., Maizlish V.E., Galanin N.E. Girichev G.V. *Int. J. Mol. Sci.* **2022**, *23*, 13922, doi: 10.3390/ijms232213922.
29. Berezin D.B. *Macrocyclic Effect and Structural Chemistry of Porphyrins [Макроциклический эффект и структурная химия порфиринов]* URSS, Krasand: Moscow, Russia, **2010**, ISBN 978–5-396–00112-1.
30. Koifman O.I., Ageeva T.A., Beletskaya I.P. *Macroheterocycles* **2020**, *13*, 311–467, doi: 10.6060/mhc200814k.
31. Becke A.D. *J. Chem. Phys.* **1993**, *98*, 5648–5653, doi: 10.1063/1.464913.
32. Becke A.D. *Phys. Rev. A.* **1988**, *38*, 3098–3101, doi: 10.1103/PhysRevA.38.3098.
33. Lee C., Yang W., Parr R.G. *Phys. Rev. B* **1988**, *37*, 785–789, doi: 10.1103/PhysRevB.37.785.
34. Grimme S. *J. Comp. Chem.* **2006**, *27*, 1787–1799, doi: 10.1002/jcc.20495.
35. Dunning T.H. Jr. *J. Chem. Phys*. **1989**, *90*, 1007–1024, doi: 10.1063/1.456153.
36. Glendening E.D., Badenhoop J.K., Reed A.E., Carpenter J.E., Bohmann J.A., Morales C.M., Weinhold F. **2004**. Available online: *http://www.chem.wisc.edu/~nbo5* (accessed on 20 March 2023).
37. Frisch M.J., Trucks G.W., Schlegel H.B., Scuseria G.E., Robb M.A., Cheeseman J.R., Scalmani G., Barone V., Mennucci B., Petersson G.A. Gaussian 09 (Gaussian, Inc., Wallingford CT), **2009**, Available online: *https://gaussian.com/glossary/g09/* (accessed on 20 March 2023).
38. Vishnevskiy Y.V., Zhabanov Y.A. *J. Phys. Conf. Ser.* **2015**, *633*, 012076, doi: 10.1088/1742–6596/633/1/012076.
39. Sipachev V.A. *J. Mol. Struct. (Theochem.)* **1985**, *121*, 143–151, doi: 10.1016/0166–1280(85)80054–3.
40. Zhurko G.A., Zhurko D.A. ChemCraft. Version 1.6, Build 312. Available online: *https://www.chemcraftprog.com/index.html* (accessed on 20 March 2023).
41. Johnson E.R., Keinan S., Mori-Sanchez P., Contreras-Garcia J., Cohen A.J., Yang W. *J. Am. Chem. Soc.* **2010**, *132*, 6498–6506, doi: 10.1021/ja100936w.
42. Lu T., Chen F. *J. Comput. Chem.* **2012**, *33*, 580–592, doi: 10.1002/jcc.22885.
43. Jeziorski B., Moszynski R., Szalewicz K. *Chem. Rev.* **1994**, *94*, 1887–1930, doi: 10.1021/cr00031a008.
44. Parrish R.M., Parker T.M., Sherrill C.D. *J. Chem. Theory Comput.* **2014**, *10*, 4417–4431, doi: 10.1021/ct500724p.
45. Parrish R.M., Gonthier J.F., Corminbeuf C., Sherrill C.D. *J. Chem. Phys.* **2015**, *143*, 051103, doi: 10.1063/1.4927575.
46. Smith D.G.A., Burns L.A., Simmonett A.C., Parrish R.M., *et al. J. Chem. Phys.* **2020**, *152*, 184108, doi: 10.1063/5.0006002.
47. Lindsey J.S., Hsu H.C., Schreiman I.C. *Tetrahedron Lett*. **1986**, *27*, 4969–4970, doi: 10.1016/S0040–4039(00)85109–6.
48. Girichev G.V., Utkin A.N., Revichev F. *Instruments and Experimental Technique [Приборы и техника эксперимента]* **1984**, *27*, 187.
49. Girichev G.V., Shlykov S.A., Revichev Y.F. *Instruments and Experimental Technique [Приборы и техника эксперимента]* **1986**, *4*, 167.
50. Girichev G.V., Shlykov S.A., Petrova V.N., Subbotina N.Y., Lapshina S.B., Danilova T.G. *Izvestiya Vysshikh Uchebnykh Zavedenii Khimiya i Khimicheskaya Tekhnologiya [ChemChemTech]* **1988**, *31(8)*, 46–51.
51. Girichev E.G., Zakharov A.V., Girichev G.V., Bazanov M. I. *Izv. Vyssh. Uchebn. Zaved., Tekhnol. Tekst. Prom.* **2000**, *2*, 142–146.
52. Vishnevski Y.V., UNEX [1.6], Available online: *https://unex.vishnevskiy.group* (accessed Mon Sep 11 2023)
53. Doms L., Geise H., Van Alsenoy C., Van Den Enden L., Schafer L. *J. Mol. Struct.* **1985**, *129*, 299–314. doi: 10.1016/0022–2860(85)80173–3.
54. Hargittai I., Chamberland B. *Comput. Math. Appl.* **1986**, *12*, 1021–1038, doi: 10.1016/0898–1221(86)90438–4.

Received 27.10.2023
Accepted 08.12.2023